CHAPTER II
THEORETICAL BACKGROUND AND LITERATURE REVIEW

Corrosion is one of the most important damage modes for engineering structure that are construct from metal. Among all the Industries that have to cope with corrosion, the power industry is one of the most vulnerable. The CANDU reactors, such as at the Point Lepreau Generating Station (PLGS), are the most seriously affected for experiencing the highest thinning rates in the piping especially in the outlet feeder pipes of the primary heat transport system.

2.1 CANDU® Nuclear Reactor

The CANDU reactor is a world leading nuclear reactor in terms of reliability and power production developed in Canada. The acronym CANDU stands for "CANada Deuterium Uranium". This is a reference to its deuterium-oxide (heavy water) moderator and its use of natural uranium fuel. Although this type of nuclear reactor originated in Canada, it has been sold and used in many countries such as Korea, Romania, Argentina, and China.

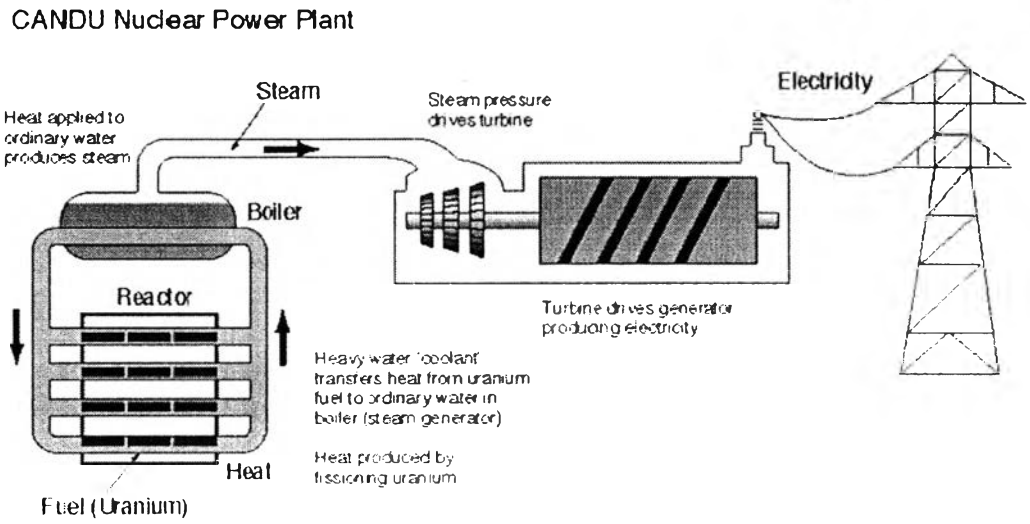

Figure 2.1 Schematic of a CANDU nuclear reactor.

A CANDU reactor uses a fission-controlled reaction which is similar to most classic nuclear power plants in design. The generated heat from the nuclear reaction is carried by the heavy water (D_2O), which is the primary coolant through carbon steel pipes and headers to the steam generator. The hot heavy water generated in this primary cooling loop is passed into heat exchangers heating light water in the less-pressurized secondary cooling loop. This water turns to steam and powers a conventional turbine which turns a generator to produce electricity. A schematic of the CANDU nuclear reactor illustrating these features is shown in Figure 2.1.

2.1.1 CANDU Primary Coolant Loop

Heavy water is the common name for D_2O, deuterium oxide. It is similar to light water (H_2O) in many ways, except that the hydrogen atom in each water molecule is replaced by heavy hydrogen, or deuterium (a non-radioactive isotope of hydrogen). The deuterium makes D_2O about 10 per cent heavier than ordinary water. Deuterium is much more efficient as a moderator than light water, thus allowing the use of natural uranium as a fuel. The deuterium separation is an added initial capital cost which, over the plant lifetime, is offset by the lower natural uranium fuel costs.

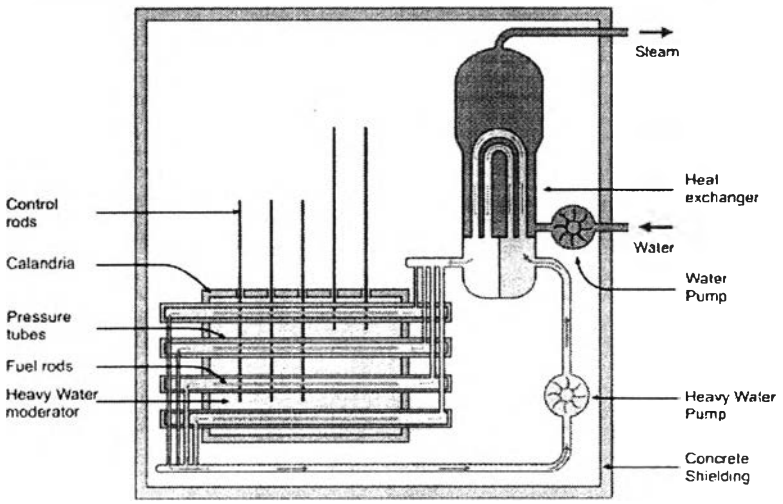

Figure 2.2 Primary coolant system of CANDU reactor (Emoscopes, 2006).

The reactor coolant circulation is called the primary coolant system as shown in Figure 2.2. The primary coolant loop consists of three main components: the steam generator, the reactor core, and the piping system. The primary coolant D_2O enters the reactor core at 265 °C to remove heat from the nuclear reaction then leaves the core at 310 °C. Chemicals are added to the coolant flow for two major requirements. The first one is to minimize dissolved oxygen by dissolving hydrogen within specification of 3-10 cm^3/kg at STP. Another reason is to maintain the alkalinity by adding lithium hydroxide to within the specification of pH (Lister *et al.*, 1998).

2.1.2 Feeder Pipe Material and Conditions

For the piping system, the material of construction is A-106 grade B carbon steel since it can be used as the construction material of CANDU feeder pipes for long term operation. Carbon steel A-106 grade B contains iron as the main component with small amounts of carbon, chromium, cobalt, manganese, nickel, copper and other elements trace. The amount of chromium in steel is an important factor in the thinning phenomenon because chromium can form an oxide that protects the surface of steel (Robertson and Forrest, 1991).

Table 2.1 Normal outlet feeder conditions at Point Lepreau Generating Station

Property	Normal Value
Temperature	307-312°C Average: 310.7 °C
Pressure	10.3 MPa
Two-phase quality	0.2-19% Average: 1.06%
Time in two-phase	0-94% Average: 49%
Average Velocity	6.5-14.5 m/s Average:12.2 m/s
pH_a	Operating 10.2-10.4 since 1996
Dissolved O_2	Specification <0.01 mg/kg
Dissolved D_2	Specification 3-10 mL(STP)/kg

The average primary heat transport system conditions over the normal range of operations are summarized in Table 2.1. It is under conditions of high temperature, high flow velocity and low dissolved oxygen concentration that outlet feeders develop their characteristic magnetite film. These conditions coupled with the under saturation of iron in the coolant, are believe to be sufficient to cause FAC and thereby produce hydrogen (Kelly *et al.*, 2007).

2.2 Coleson Cove Generating Station

Coleson cove is an oil fired generating station located in New Brunswick, Canada. It went in service since 1976 with a full power of 978 MW. The heat from burning fossil fuels is converted to electricity by using steam generators. Wall thinning due to corrosion in utility boiler water-wall tubing is a significant operational concern for boiler operators.

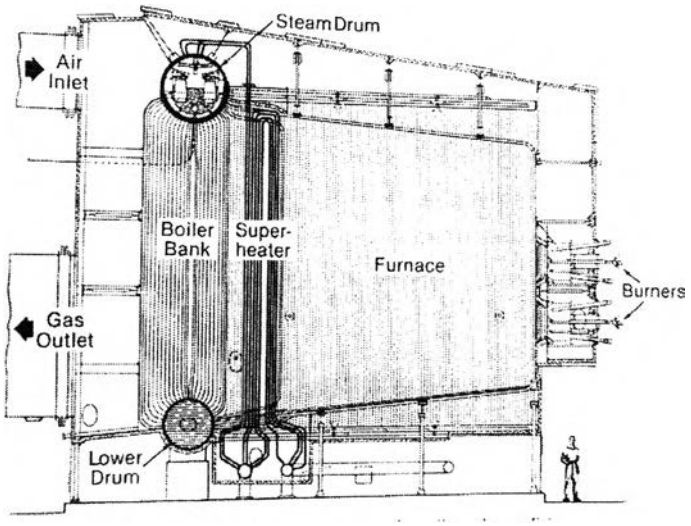

Figure 2.3 Integral furnace industrial boiler for oil and gas firing (Babcock and Wilcox, 1972).

2.2.1 Steam Generators

Steam generators, or boilers, use heat to convert water into steam for a variety of applications such as electric power generation and industrial process heat-

ing. Technical and economic factors indicate that the most effective way to produce high pressure steam is to heat relatively small diameter tubes containing a continuous flow of water. Subcooled water enters the tube to which heat is applied. As the water flows through the tube, it is heated to its boiling point, bubbles are formed, and wet steam is generated. In most boilers, a steam-water mixture leaves the tube and enters a large vessel (steam drum) where steam is separated from water. The remaining water is then mixed with the replacement water and returned to the heated tube (Babcock and Wilcox, 1972).

2.2.2 Boiler Water Walls Tubing

Boiler surface is defined as the tubes, drums and shells which are part of the steam-water circulation system and which are in contact with the hot gases. While boilers can be classified as shell, fire tube and water tube types, modern high capacity boilers are of the water tube types which allows greater boiler capacity and higher pressure than the other types. In the water tube boiler, the water and steam flow inside the tubes and the hot gases flow over the outside surfaces (Babcock and Wilcox, 1972).

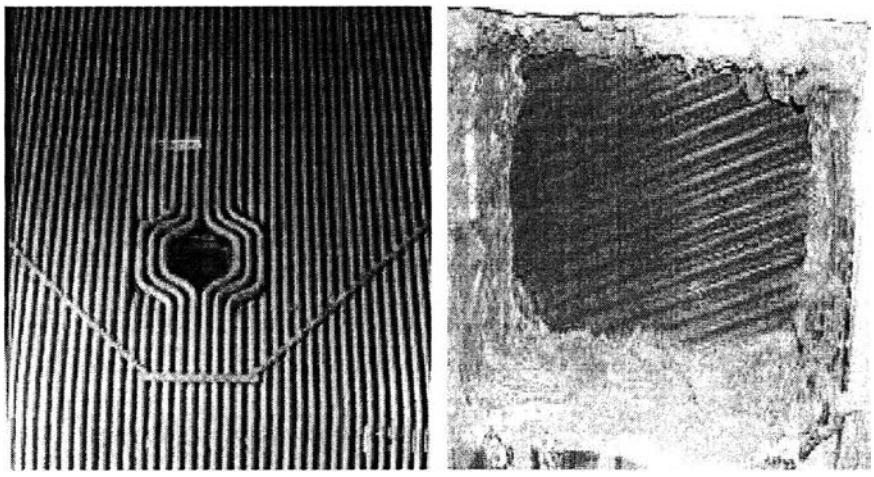

Figure 2.4 Boiler water walls tubing.

In a large plant, the furnace temperature is quite high and consequently, the refractory material may get damaged. In such cases, refractory walls are

made hollow and air is circulated through hollow space to keep the temperature of the furnace walls low. The recent development is to use water walls as shown in Figure 2.4. These tubes form the walls of the boiler and are hence called water walls or water wall panels. The water walls have advantages due to the following reason. First of all, these walls provide a protection to the furnace against high temperature. They avoid the erosion of the refractory material and insulation. Besides the evaporation capacity of the boiler is increased.

2.2.3 Boiler Blowdown

Boiler water always contains dissolved minerals and solids which will accumulate within the boiler system. These minerals and solids must be removed to prevent blocked connections, impaired heat transfer, hot spot or boiler damage. The purpose of boiler blowdown is to control the dissolved solids of the recirculating water. It reduces the concentration of solid corrosion products (metal oxides). Blowdown protects boiler surfaces from severe scaling or corrosion problems that can result otherwise.

2.3 Corrosion of Steel

2.3.1 Definition of Corrosion

Corrosion is defined as the destruction or deterioration of a material because of reaction with its environment. Higher temperatures and pressures usually involve more severe corrosion conditions. In industry when the corrosion occurs, it does not only damage the equipment but also affects its working efficiency, expense, and safety in the plant. However, corrosion is a beneficial or desirable in some cases. For example, anodizing of aluminum is a beneficial corrosion process used to obtain better and more uniform appearance in addition to the protective corrosion product on the surface (M. G. Fontana, 1986).

2.3.2 Corrosion of Steel in Water System

The corrosion of metals in an aqueous system involves two or more electrochemical reaction. Carbon steel corrosion can be represented by two simple

reactions as the following,

Anodic reaction: $$Fe \rightarrow Fe^{2+} + 2e^{-} \quad (2.1)$$

Cathodic reaction: $$2H_2O + 2e^{-} \rightarrow H_2 + 2OH^{-} \quad (2.2)$$

Iron metal is corroded and converted to iron ions, ferrous (Fe^{2+}), formed at the anodic surface. In deaerated solution or solution without air, hydrogen molecules are formed at the cathodic surface. In slight alkaline and in the absence of oxygen; the condition in the primary coolant system of a CANDU reactor, the oxide of metal produced from the corrosion process is predominately magnetite, Fe_3O_4 as shown below (Taenumtrakul, 2004).

$$3Fe + 4H_2O \rightarrow Fe_3O_4 + 4H_2 \quad (2.3)$$

Therefore, it can be concluded that in high temperature water, iron can be corroded and forms a magnetite oxide film, Fe_3O_4, covering the metal surface.

2.3.3 Flow-Accelerated Corrosion (FAC)

Flow-Accelerated Corrosion (FAC) or Flow-Assisted Corrosion is one form of corrosion which is defined as the acceleration or increase in the rate of deterioration or attack on the metal because of the relative movement between the corrosive fluid and the metal surface (Fontana, 1986). A magnetite oxide film formed on the carbon steel surface protects the surface by limiting the diffusion processes. In FAC process, a protective oxide layer on a metal surface dissolves from the surface as dissolved iron, or forms a solid corrosion product which is mechanically swept from the metal surface. The underlying metal corrodes to re-create the oxide, and thus the metal loss continues as shown in Figure 2.5. The oxide film formation at the metal surface equals its dissolution at the oxide-coolant interface, at steady state. An increase in the fluid velocity can increase the flux of removed oxide to the bulk coolant. Therefore, the rate of FAC depends on the flow velocity. FAC often affects carbon steel piping carrying ultra-pure, deoxygenated water or wet steam.

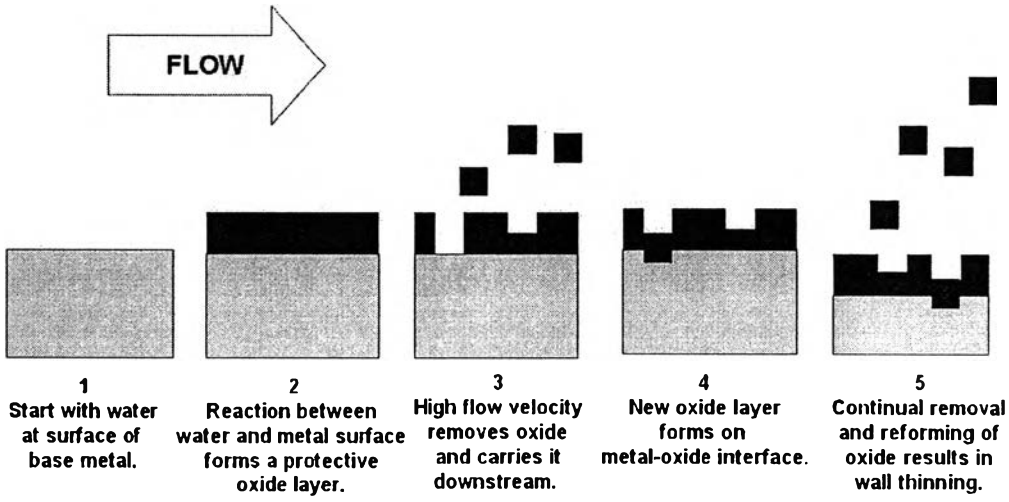

Figure 2.5 Simplified mechanism for FAC (M. D. Silbert, 2002).

Lister *et al.* (1998) explained the effect of FAC on the carbon steel oxide film formed in high temperature water. It is confirmed that the oxide film formed on the carbon steel limits the corrosion, and is mainly composed of magnetite (Fe_3O_4). FAC can be described by two processes in series. The first one is magnetite film dissolution followed by mass transport of the dissolved iron to the bulk coolant. If the coolant is under saturated in dissolved iron, dissolution of the oxide layer to the bulk coolant will occur and cause the oxide film to be reduced. By increasing the fluid velocity, the mass transport of iron ions to the bulk solution can be increased which results in a higher mass transfer coefficient and the flux of iron ions into the bulk coolant. Thus, if the mass transfer of iron ions emerging from pores at the oxide-coolant interface to the bulk coolant is faster than oxide precipitation, no outer layer will form. At steady-state, the oxide formation at the metal-oxide interface equals its dissolution at the oxide coolant interface.

2.3.4 FAC on the Feeder Pipe of CANDU Reactor

The FAC effect can be investigated in the primary heat transfer circuit of the CANDU reactor. The outlet feeder pipes experience more FAC than inlet feeder pipes, since the coolant temperature rises from 265 to 310 °C during flow through the reactor core, where there is no source of iron, resulting in higher solubil-

ity of the oxide film. Consequently, the inlet feeder pipes carry the saturated coolant with dissolved iron, which results in a lower corrosion rate and a relatively thick oxide film compared with outlet feed pipes.

2.4 The Effect of Temperature on the Corrosion Rate

The corrosion rate of metals is known to conform to the kinetic Arrhenius equation. However, anomalies in the form of breaks are observed on the temperature-dependence curves of the corrosion rate since the structure of the metal changes with temperature.

Figure 2.6 shows the effect of temperature on the corrosion rate of carbon steel in mildly alkaline deaerated water (Chexal *et al.*, 1996). The graphs show that at low temperature, the corrosion rate increases with an increase in temperature. The corrosion rate is largest in the range of 130-140 °C. At further increase in temperature results in a reduction of the corrosion rate. The corrosion rate increase as the temperature increases in the low temperature range because the formation of a protective oxide layer has is not formed. At higher temperatures, the corrosion rate decreases. It can be explained by transition of the materials to the passive state (É. T. Shapovalov, 1994). Figure 2.7 shows the oxide film structure in different conditions.

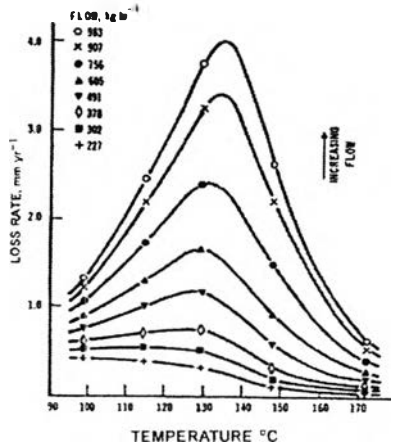

Figure 2.6 Flow and temperature dependence of single-phase FAC for an ammonia solution with a room temperature of 9.04 (Chexal *et al.*, 1996).

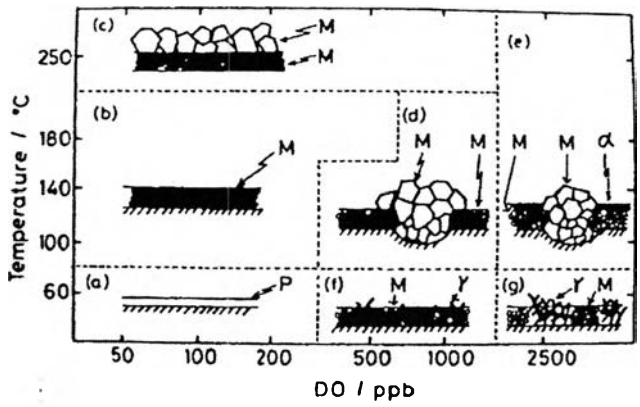

Figure 2.7 Temperature and dissolved oxygen (DO) diagram (K. Mabuchi, 1991).

From extrapolating the curves in Figure 2.6, it is observed that at temperatures more than 200 °C, the rate of corrosion should be quite low. This would contradict the generally accepted that the corrosion is severe at high temperature in alkaline systems.

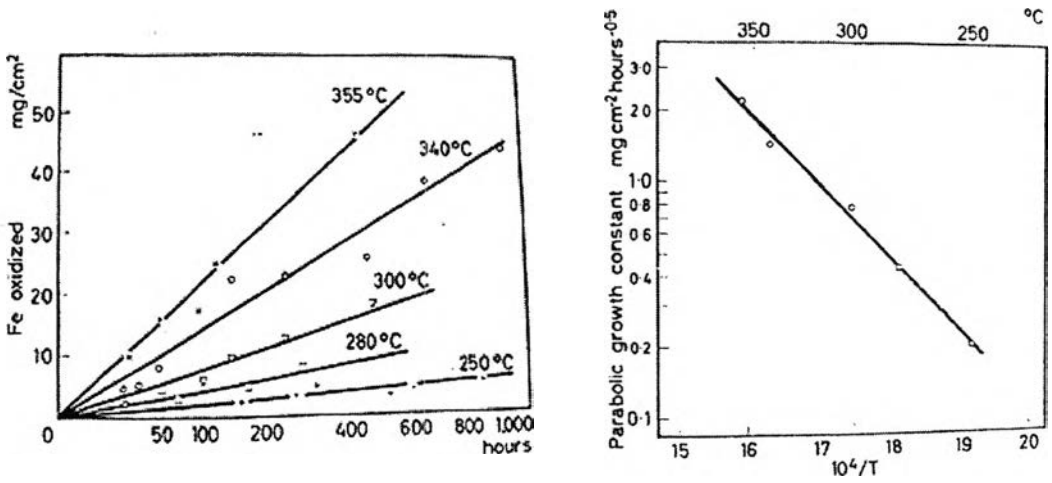

Figure 2.8 Oxidation of mild steel in 13% NaOH at five different temperatures plotted against square root time is on the left. and on the right shows variation with reciprocal absolute temperature of logarithm of the parabolic growth constant (Potter and Mann. 1962).

However, Potter and Mann (1962) studied corrosion rates of unstressed mild steel in static alkaline solution at 250-355 °C. The results indicated that increasing temperatures accelerate the corrosion of steel under these conditions. The parabolic rate constants for each temperature have been calculated, and are logarithmically plotted against the reciprocal of absolute temperature as shown in Figure 2.8. The linearity of the relation suggests that the corrosion process conforms to a kinetic equation of the usual exponential form. Therefore a further increase of corrosion rate at higher temperature is caused by the effect of a temperature factor, and not by repassivation.

The solubility of iron at different pH and temperature was reported by Sweeton and Baes (1970). For operating conditions at a pH_{25} of approximately 10, this condition is located at the bottom right-hand corner of Figure 2.9. The diagram indicates that the solubility of magnetite increases with an increase in temperature, as there is a positive slope in this region as a pH of 10 (L.L. Lang, 1996). Thus, higher temperature results in increasing solubility of ferrous iron in the solution, and increasing the mass transfer.

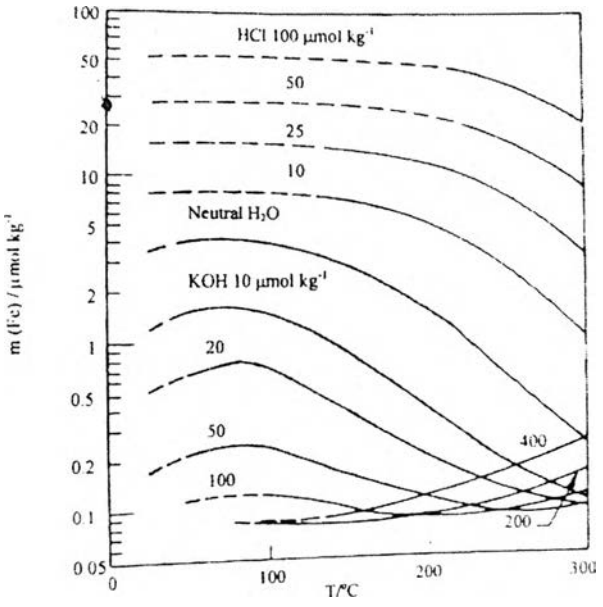

Figure 2.9 Sweenton and Baes iron solubility results (L.L. Lang, 1996).

In 1994, É. T. Shapovalov studied the temperature dependence of the corrosion rate of metallic materials in acid solution over a large temperature range. The graph, as shown in Figure 2.10, contains ranges in which the corrosion rate decreased with increase in temperature as a result of passivation of the metal. At lower and higher ranges of temperature, the corrosion rate increase with increase in temperature by the influence of solubility and mass transfer.

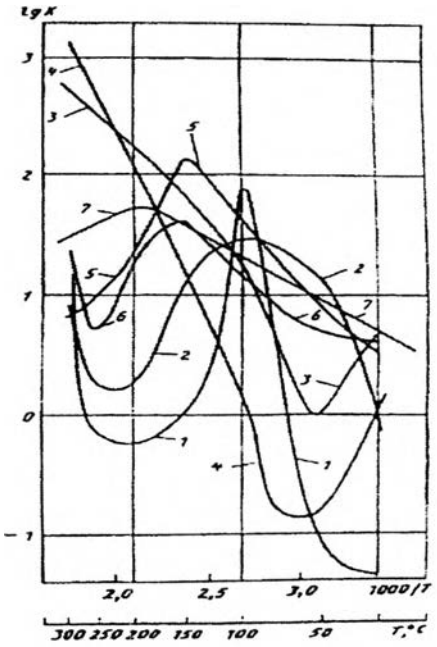

Figure 2.10 Dependence of the corrosion rate of metals steels, and alloys on temperature of concentrated sulfuric acid (É. T. Shapovalov, 1994).

2.5 Corrosion Mechanism and Hydrogen Evolution

2.5.1 Mechanism of Oxide Growth

Magnetite (Fe_3O_4) is the structure of iron oxide that is observed on a metal surface such as carbon steel in CANDU reactor. This type of oxide film behaves like a corrosion resistance film to protect the steel matrix from the corrosive environment. The morphology of the oxide film is influenced by the chemical composition of the alloy, exposure conditions and surface finishing (Lister *et al.*, 1994).

The corrosion of carbon steels in high-temperature water, in the absence of oxygen, involves the transport of oxygen-bearing species to the metal/oxide interface and the outward movement of metal ions to the solution phase. When the solution phase becomes saturated with soluble iron, an outer magnetite layer is nucleated and grows on the surface. The net result is a double magnetite layer (Cheng and Steward, 2004). The first one is an inner oxide layer. The morphology of this layer is small crystal, compact and adherent since it nucleates in the confined space and grows at the metal/oxide interface, replacing the corroded volume. Another layer is an outer oxide layer. This layer is composed of coarse octahedral crystals since it grows by outward diffusion of the metal ions, especially iron, along oxide grain boundaries without volume constraint (Potter and Mann, 1992). The schematic of oxide layer of carbon steel corroding in coolant under-saturated dissolved iron is shown in Figure 2.11. SEM surface of oxide film formed under flow condition is shown in Figure 2.12.

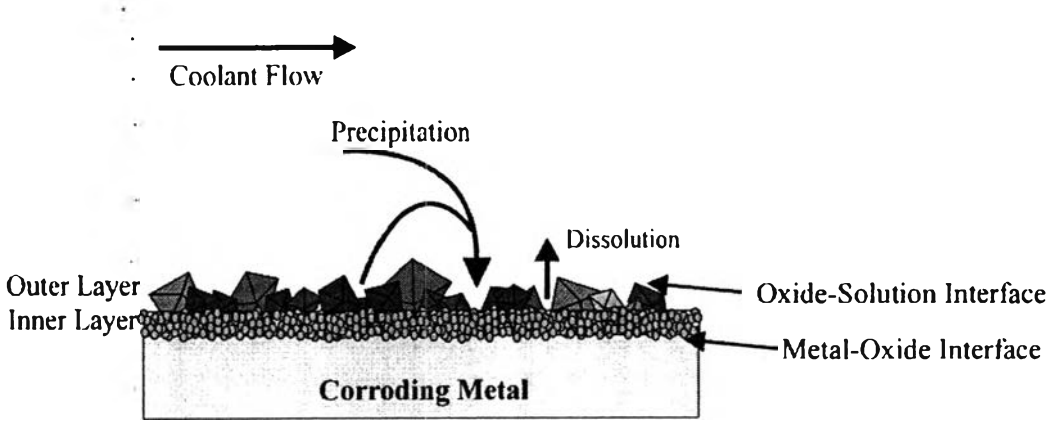

Figure 2.11 Schematic of carbon steel corroding in coolant under-saturated in dissolved iron (Lister *et al.*, 2001).

The outer layer normally consists of magnetite Fe_3O_4 which can also contain nickel. The inner layer consists of a chromium-rich spinel. The alloying elements of the steel pass congruently into the oxide film because its growth rate is much higher than diffusion rates of the relevant alloying elements in the metal. According to the diffusion rates of the metal ions in the spine lattice Cr and Ni move

more slowly than Fe and are retained and thus enriched in the inner layer (B. Stellwag, 1998).

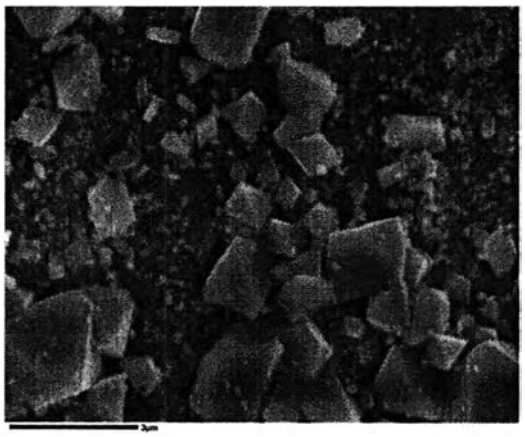

Figure 2.12 SEM of oxide film formed under flow condition at 10,000X magnification (T. Pattanaparadee, 2007).

Cheng and Steward (2004) investigated the oxygen-bearing species in high-temperature deaerated alkaline solution. They proposed that in the absence of oxygen, the inward movement of oxygen-bearing species occurs by diffusion of either water molecules or oxygen ions or hydroxide ions. Since oxygen ions involve the formation of oxide film only after a sufficiently anodic potential is imposed and a de-protonation of H_2O takes place. Therefore, oxygen ions cannot be the diffusion species in the reported experiments. In addition, it is expected that the steel would be negative with respect to the solution because of the injection of Fe^{2+} or $Fe(OH)^{+}$ into the water.

Considering the thin thickness of the film, the electric charge strength across the film is very high. The established electric field will block the negatively charged ions, such as OH^- from moving towards the steel surface. This eliminates hydroxide ions as the diffusion species. Therefore, the oxygen-bearing species involving the formation of the magnetite layer must be water. They also suggested a schematic view of the magnetite film formed on a steel surface in high-temperature water solution as shown in Figure 2.13.

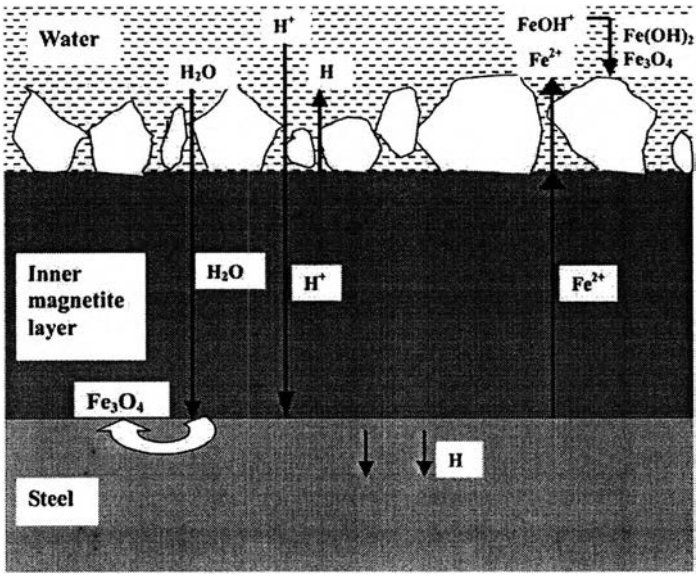

Figure 2.13 A schematic view of the formation mechanism of the magnetite film on the steel surface in high-temperature water (Cheng and Steward, 2004).

Water molecules diffuse through the inner oxide layer and react directly with steel at the steel/oxide interface. Iron dissolution occurs where no oxide layer exists. Protons at the oxide/water interface diffuse through the oxide layer to consume the electrons produced by anodic reactions and discharge as hydrogen atoms at the steel/oxide interface. The relevant reactions occurring at the steel/oxide interface are shown below.

$$3Fe + 4H_2O \rightarrow Fe_3O_4 + 8H^+ + 8e^- \quad (2.4)$$

$$Fe \rightarrow Fe^{2+} + 2e^- \quad (2.5)$$

$$H^+ + e^- \rightarrow H \quad (2.6)$$

The ferrous ions diffusing out of the oxide layer exist as $Fe(OH)^+$ in high-temperature water must stabilize themselves by decreasing their charge/radius ratios through hydrolysis to form hydrous iron ions. The hydrous iron ions will deposit as loose $Fe(OH)_2$ once the saturation of iron ions is achieved. The outer deposition of the magnetite layer is then formed in high-temperature water, accompanying the discharge of hydrogen ions. Therefore, the electrochemical reactions occurring at the oxide/water interface are,

$$3Fe(OH)^{+} + H_2O \rightarrow Fe_3O_4 + 5H^{+} + 2e^{-} \quad (2.7)$$

$$2H^{+} + 2e^{-} \rightarrow H_2 \quad (2.8)$$

The reactions above confirmed that hydrogen is produced in the carbon steel corrosion process.

2.5.2 Hydrogen Emission during Steel Corrosion

Tomlinson (1981, 1989) studied the hydrogen emission from the oxidation of steel. He reported that protons produced from the corrosion process diffuse in both directions across the oxide, with the direction and magnitude of the proton flux being dependent on the structure of oxide layer. Hydrogen atoms are formed at both the metal/oxide interface and the oxide/water interface. At the oxide/water interface, hydrogen atoms are either discharged at the oxide/water interface by electron diffusion across the oxide or diffusion through the oxide as protons which are discharged at the metal/oxide interface. Under the concentration and potential gradient, protons at the oxide/water interface diffuse rapidly through the oxide layer and discharge as hydrogen atoms at the metal/oxide interface.

The experimental evident indicates that up to 90% of the hydrogen atoms are generated at the metal/oxide interface during the corrosion of carbon steels by high temperature deaerated water. More than 99% of these hydrogen atoms will diffuse through the metal at the temperature of interest since hydrogen diffuse through the metal 330 times more quickly than through the oxide. It is suggested that if the rate of growth of the inner layer/ rate of growth of the outer layer is constant, then the ratio of hydrogen emission from metal and oxide surfaces should also be constant. Furthermore, the fraction of hydrogen passing through the steel appears to increase with the amount of oxide deposited on the tube surface.

2.6 The Fundamental Law of Diffusion

Diffusion is the movement of particles from an area where their concentration is high to an area that has low concentration. In the crystal solid state, the occurrence of diffusion is upon the availability of point vacancies throughout the crystal

lattice. Since the prevalence of point vacancies increases in accordance with the Arrhenius equation, the rate of crystal solid state diffusion increases with temperature (G. Paul, 1963).

Effusion, on the other hand, is the movement of gas through a tiny opening or semi-permeable membrane into lower pressure or vacuum as shown in Figure 2.14. This will occur if the diameter of the hole is considerably smaller than the mean free path of the molecules. However, this movement is also through random gas molecule motion, that is, through the same mechanism that drives diffusion.

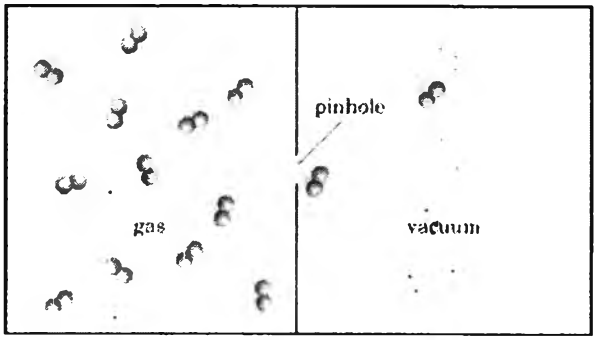

Figure 2.14 Effusion of gas through a tiny pore or pinhole into a vacuum.

2.6.1 Fick's Law of Diffusion

The laws of diffusion connect the rate of flow of diffusing substance with the concentration gradient. Fick's Law is a mathematical description used to describe diffusion, and define the diffusion coefficient, D.

2.6.1.1 Fick's First Law

Fick's First Law is used in steady-state diffusion, for example when the concentration within the diffusion volume does not change with respect to time of flux. The diffusion model can be described as

$$\text{Hydrogen Flux} = D\frac{(\textit{hydrogen conc. at } x=0)-(\textit{hydrogen conc. at } x=l)}{(\textit{thickness at } x=l)-(\textit{thickness at } x=0)} \qquad (2.9)$$

or, symbolically,

$$J = D\frac{c|_{x=0}-c|_{x=l}}{l-0} \qquad (2.10)$$

Where J is the diffusion flux or the quantity of substance per area per time, D is the diffusion coefficient or diffusivity [length^2 time^{-1}], c is the concentration of the diffusing substance given as amount of substance per volume, x is the coordinate chosen perpendicular to the reference surface.

The distance l is that over which diffusion occurs. In differential form can be rewritten as follow.

$$J = -D\frac{\partial c}{\partial x} \tag{2.11}$$

D is proportional to the velocity of the diffusing particles, which depends on the temperature, viscosity of the fluid and the size of the particles. In steady state, Fick's First Law can be integrated to give

$$J = D\frac{(c_1 - c_2)}{l} \tag{2.12}$$

where c_1 and c_2 are the concentrations of penetrant at the feed and permeate sides, respectively, and l is the thickness of the diffusion path.

2.4.1.2 Fick's Second Law

Fick's Second Law is used in non-steady or continually changing state diffusion, for example when the concentration within the diffusion volume changes with respect to time. The differential equation of Fick's Second Law is shown below.

$$\frac{\partial c}{\partial t} = D\frac{\partial^2 c}{\partial x^2} \tag{2.13}$$

It can be derived from the Fick's First Law and the mass balance,

$$\frac{\partial c}{\partial t} = -\frac{\partial}{\partial x}J = \frac{\partial}{\partial x}\left(D\frac{\partial}{\partial x}c\right) \tag{2.14}$$

Assuming the diffusion coefficient D to be a constant we can exchange the orders of the differentiating and multiplying on the constant,

$$\frac{\partial}{\partial x}\left(D\frac{\partial}{\partial x}c\right) = D\frac{\partial^2 c}{\partial x^2} \tag{2.15}$$

and, thus, receive the form of the Fick's equations as was stated above. For the case of 3-dimensional diffusion Fick's Second Law becomes,

$$\frac{\partial c}{\partial t} = D\nabla^2 c \tag{2.16}$$

where ∇ is the del operator.

Finally if the diffusion coefficient is not a constant, but depends upon the coordinate and/or concentration, the Fick's Second Law becomes,

$$\frac{\partial c}{\partial t} = \nabla \cdot (D\nabla c) \tag{2.17}$$

For the steady states, when concentration does not change with time, the left part of the above equation will be zero. Therefore in one dimension and when D is constant, the solution for the concentration will be the linear change of concentrations along x.

2.6.2 Henry's Law and Sievert's Law

In some practical systems, the surface concentration of the gas is not known, but only the gas or vapor pressure on the two sides of the membrane. In this case Henry's Law is used.

$$S_H = \frac{C_{gas}}{P_{gas}} \tag{2.18}$$

Where S_H is a constant relating the vapor pressure of a nondissociative gas into its concentration in a liquid or solid at dilute concentration, i.e., the solution phase. C_{gas} is the concentration of gas in the solvent. and P_{gas} is the pressure of the gas over the solvent. Under the assumption that there are no surface effects on both sides of the specimen the hydrogen surface concentration will be equal to the solubility limit for hydrogen in that metal. Since the inlet and outlet pressure of the gas can usually be measured, pressure is substituted for concentration into Fick's First Law, via Henry's Law. The Henry's Law constant is in fact the solubility constant S, which expresses concentration per unit of pressure.

Henry's Law should not be used when there is dissociation or reaction in either phase. A common example is the dissociation of diatomic molecules (hydrogen, oxygen, nitrogen), when they dissolve in a liquid or solid metal. A modification of Henry's Law is required. Hydrogen solubility in metals is a function of the half-power of the partial pressure due to the dissociation of the hydrogen molecules.

This is called Sievert's Law. Thus the driving force for mass transfer of a diatomic gas across a metal is proportional to the difference in square roots of the partial pressures in the contacting gas (R.A. Oriani, 1993).

$$S_H = \frac{C_H}{p_{H_2}^{1/2}} \tag{2.19}$$

The Sieward's Law constant is also called solubility. Substitution of equation 2.19 into equation 2.11 yields,

$$J = -DS\frac{\partial p_{H_2}^{1/2}}{\partial x} \approx -DS\frac{\Delta p_{H_2}^{1/2}}{\Delta x} \tag{2.20}$$

In this case, $\Delta p_{H_2}^{1/2}$ is the square root of the pressure difference of the diffusing gas across a membrane, and Δx is the thickness of the membrane. The negative sign represents the direction of diffusion.

In accordance with this law, a linear relation is often found between rate of permeation and the square root of the pressure. This indicates that not molecules, but rather free atoms, are diffusing through the metal. There are however exceptions to this relation. It was observed that a linear relation between $\sqrt{p}$ and the rate of permeation applies for sufficiently high pressures only, while for the lowest pressure employed, this relation breaks down. W. Jost (1960) suggested that the simple square root law can be expected to hold only if these reactions at phase boundaries are very fast compared with the diffusion through the membrane. Deviations will be more marked at the lower temperature.

Equation 2.20 can be rearranged to correspond to the usual representation of data, where the total amount of the gas has permeated the membrane, q(mol), is plotted as a function of time. Equation 2.20 then becomes

$$q = Qt = JAt = DS\frac{A}{\Delta x}\Delta p_{H_2}^{1/2} \cdot t \tag{2.21}$$

Where A is the slab area, Q is the amount of the gas permeated the membrane per unit area and t is the time since reaching steady state. As time passes, the hydrogen permeates through the metal and when the steady-state condition is reached, the concentration gradient of hydrogen through the specimen will be linear. Then, the following definition applies,

Permeability (ϕ) = diffusivity (D) × solubility (S) (2.22)

The slope of this line (dq/dt), the steady state flow rate, includes the permeability, which is specific for a given membrane material. However, the permeability constant is a much less fundamental constant than the diffusion coefficient which is expressed in units of cm^2/s, particularly as different investigators use different definitions of permeability. By differentiating Equation 2.21 and substituting ϕ from Equation 2.22,

$$\frac{dq}{dt} = \phi \frac{A}{\Delta x} \Delta p_{H_2}^{1/2} \tag{2.23}$$

The permeability (ϕ) may be calculated by knowing the steady-state flow rate, the area and thickness of the sample, and the hydrogen pressure differential across the sample, A plot of q vs. t should be a straight line at steady state, from which ϕ may be easily calculated (S.A. Steward, 1983). However, if the permeability is reduced by a surface defect, then the solubility term changes to the surface concentration (D.G. Matei, 1999).

2.6.3 Arrhenius Equation

The Arrhenius equation is an expression for the temperature dependence of the rate constant k of chemical reactions on the temperature T (in Kelvin) and activation energy E_a, as shown below

$$k = k_0 \cdot e^{\frac{-E_a}{RT}}, \tag{2.24}$$

where k_0 is the pre-exponential factor which is identical to those of the rate constant,

R is the gas constant,

E_a is the activation energy,

T is the temperature [absolute temperature] (Kelvin or degrees Rankin).

In case of the diffusion coefficient at different temperatures, Arrhenius's Law is often found to give a good prediction of the variation of the diffusion coefficient with temperature as shown in Equation 2.25.

$$D = D_0 \exp\left(\frac{-E_D}{RT}\right). \tag{2.25}$$

where D_0 is the maximum diffusion coefficient (at infinite temperature) which is obtained from a plot of natural log of D vs. $\frac{1}{kT}$, called an Arrhenius plot. The slope gives E_D and the projection to infinite $\left(\frac{1}{T} \rightarrow 0\right)$ gives $\ln D_0$ as shown in Figure 2.15.

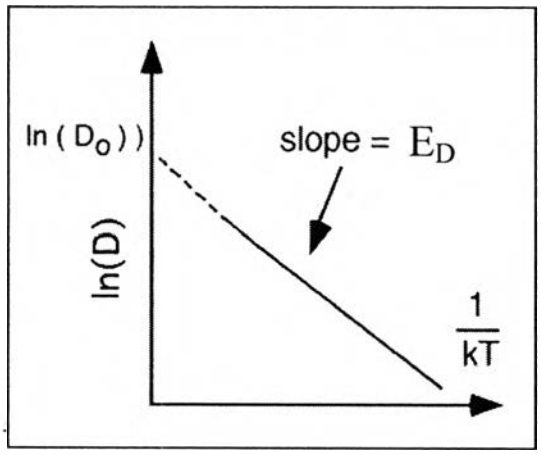

Figure 2.15 Arrhenius plot of diffusion constant.

Solubility and permeability are temperature dependent like the diffusivity and can be represented by an Arrhenius equation as followed.

$$S = S_0 \exp\left(\frac{-E_S}{RT}\right) \tag{2.26}$$

$$\phi = \phi_0 \exp\left(\frac{-E_\phi}{RT}\right) \tag{2.27}$$

Where $$\phi_0 = D_0 S_0 \tag{2.28}$$

And $$E_\phi = E_D E_S \tag{2.29}$$

2.6.4 Graham's Law of Effusion

Graham's Law of effusion was formulated by Thomas Graham. He found experimentally that the rate of effusion of a gas through a porous material is inversely proportional to the square root of the mass of its particles. This formula can be written as follow.

$$\frac{rate1}{rate2} = \sqrt{\frac{M_2}{M_1}} \tag{2.30}$$

where rate1 is the rate of effusion of the first gas

rate2 is the rate of effusion for the second gas

M_1 is the molar mass of the first gas

M_2 is the molar mass of the second gas.

According to Graham's Law, the rate at which gases effuse is dependent on their molecular weight; gases with a lower molecular weight will effuse more rapidly than gases with a higher molecular weight. Lighter molecules will have a higher velocity. This will result in more molecules passing through the hole per unit time. Figure 2.16 demonstrates the time required for different gases to diffuse through a pin hole into a vacuum.

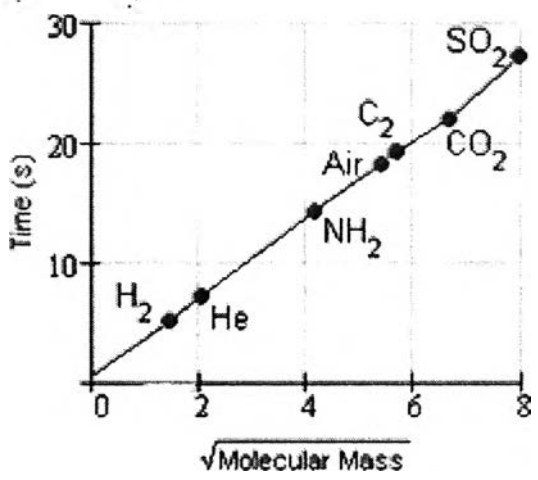

Figure 2.16 The time required for different gasses to diffuse through a vacuum.

Comparing the permeation rate of hydrogen and deuterium, there is an agreement in the results of different observers that the rate of permeation of hydrogen through palladium is higher than that of deuterium. the ratio ranging from about 1.2 to 2.5. depending on the temperature and observer.

2.7 Hydrogen Diffusion through Metal

In 1866, Graham noticed that palladium can absorb large quantities of hydrogen. At present, it is well established that hydrogen can enter into a variety of metals and alloys (P. Zoltowski, 2007). Hydrogen has a very large mobility in transition metals especially in Pd, α-Fe, V and Nb. Hydrogen dissolved in metals at low concentrations exhibits a linear relation between the concentration and the half power of the pressure, p, of the molecular gas. This is proof that hydrogen dissociates when it enters the metal (R.A. Oriani, 1994). It was reported that at a temperature higher than 298 K (25 °C), hydrogen in its stable molecular form (H_2) cannot penetrate the steel. Thus hydrogen absorbs dissociatively in metal.

2.7.1 Mechanism of Hydrogen Transport through Metal

Oriani (1994) described the absorption of hydrogen into the lattice of a metal from a molecular gas. This process must be preceded by adsorption of the molecule on the surface, dissociation into absorbed atoms, surface penetration of the absorbed atoms, and diffusion of atomic hydrogen into the bulk of material. Each of these steps is strongly affected by the atomic-scale topography of the surface and by the quantity and distribution of impurity species.

In addition to its diffusion through the bulk metal, the permeation of hydrogen through steels involves its entrance at one surface and its exit at the other surface of the specimen. There are seven steps that take place before the hydrogen is detected on the output side of the specimen. Figure 2.17 shows the seven steps that take place in the permeation of a hydrogen isotope through a metallic membrane.

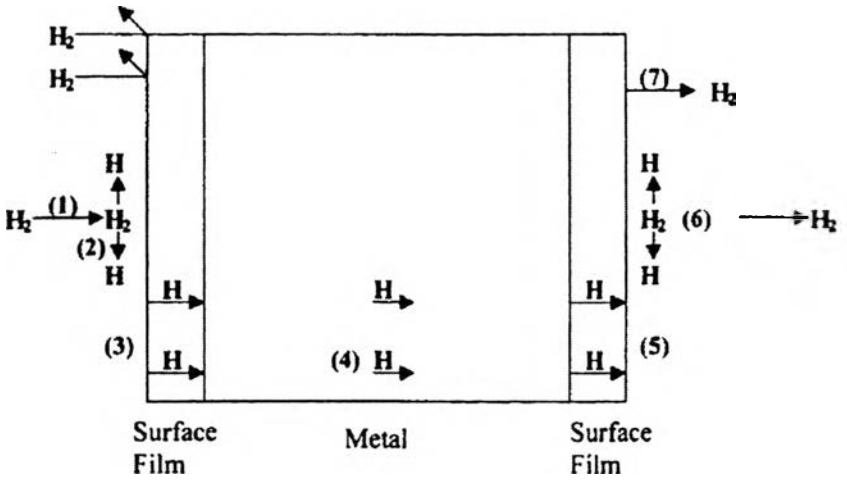

Figure 2.17 Seven steps of hydrogen permeation (M.G. Matei, 1999).

This model takes into account the presence of surface films on both the input and output side of the specimen. The seven steps are (M.G. Matei, 1999),

1. Adsorption of hydrogen molecule on the surface.
2. Dissociation of the adsorbed molecule on the surface.
3. Permeation of dissociated atoms through the surface film (oxide).
4. Permeation of atoms through the metal.
5. Permeation of atoms through the film on the output side.
6. Reassociation of atoms to form H_2 molecule.
7. Desorption of the reassociated H_2 molecule.

If hydrogen is presented to the metal surface by electrochemical deposition or by means of a partially dissociated and/or ionized hydrogen gas, the dissociation step is avoided. Therefore in the case of corrosion, hydrogen is produced as hydrogen atoms which directly absorb and diffuse through the steel.

2.7.2 Hydrogen Diffusivity Determination Methods

For the determination of diffusivity D. the generally used methods are as followed (J. Flis, 1991).

2.7.2.1 Steady-State Flow Method

This method allows the calculation of D from the experimental values of the steady-state rates of hydrogen permeation P_∞ through a metal layer, provided that the solubility, S or concentration, c of the gas in the material studied is known under the conditions of the experiment.

2.7.2.2 Hydrogen Absorption

Measurements of hydrogen absorption or desorption rates are used for the determination of D, particularly at high temperatures. Solutions of the diffusion equations under suitable initial and boundary conditions yield simple formulae for the determination of D values.

2.7.2.3 Time Lag Method

The classical time lag method consists of measuring the quantity of gas which diffuses through a metal layer of a known thickness in time t and determining from this the time lag, t_L. The diffusivity of hydrogen is estimated from the formula, $D = l^2 / 6t_L$. If the hydrogen permeation rate is measured as a function of time, the time lag t_L then equals the time after which $P = 0.63P_\infty$.

2.7.2.4 Electro Chemical Method

Application of the electrochemical method for the measurement of permeation has allowed the development of a number of new techniques for the determination of the diffusivity of hydrogen. One of these is the method of standardized curves of the absorption and desorption of hydrogen permeation rate with time which occur after the cathodic polarization current is switched on and off respectively. An advantage of this method is that D can be evaluated for various concentrations of the diffusing gas from a single experimental curve of the rise or decay of the hydrogen permeation with time.

2.7.2.5 Internal Friction Method

The internal friction method, which is based on the view that the diffusivity value for hydrogen at low temperatures, can be found from a study of the internal friction of hydrogen-charged iron specimens as a function of temperature.

2.7.2.6 Hydrogen Microprint Technique (HMT)

Hydrogen Microprint Technique is one of the hydrogen visualization methods. It utilizes a reduction effect of hydrogen atoms released from the specimen surface, and hydrogen exit sites are visualized as silver particles reduced by hydrogen. When hydrogen atoms are released from the specimen surface, they reduce silver ions in the crystals to metallic silver. After the remaining crystals are dissolved in a photographic fixing solution, hydrogen exit sites can be visualized as silver particles. This technique employs more precise observation of the hydrogen diffusion path in steel samples. However, it is impossible to measure directly the amount of hydrogen released in the HMT test, the electrochemical hydrogen permeation method is used under the same charging conditions as the HMT test (K. Ichitani *et al.*, 2003).

2.7.3 Hydrogen Diffusivity in Iron

Hydrogen diffusion in steels and alloys is complicated because of the complex microstructure. However, many works have been reported on the diffusivity of hydrogen through the membranes of iron and its alloys. The rate of hydrogen entry is very much influenced by many variables, such as the nature of the metal or alloy, its composition, thermal-mechanical history, presence of surface layers, presence of impurity, diffusion measuring method, temperature, pressure, etc (D.G. Matei, 1999).

The dependence of the diffusivity, D, of hydrogen on temperature, T, can be described in terms of the Arrhenius equation; $D = D_0 \exp(-E_D / RT)$. Plots of the hydrogen diffusion coefficient in an α-iron as a function of temperature from various references are shown in Figure 2.18 and 2.19.

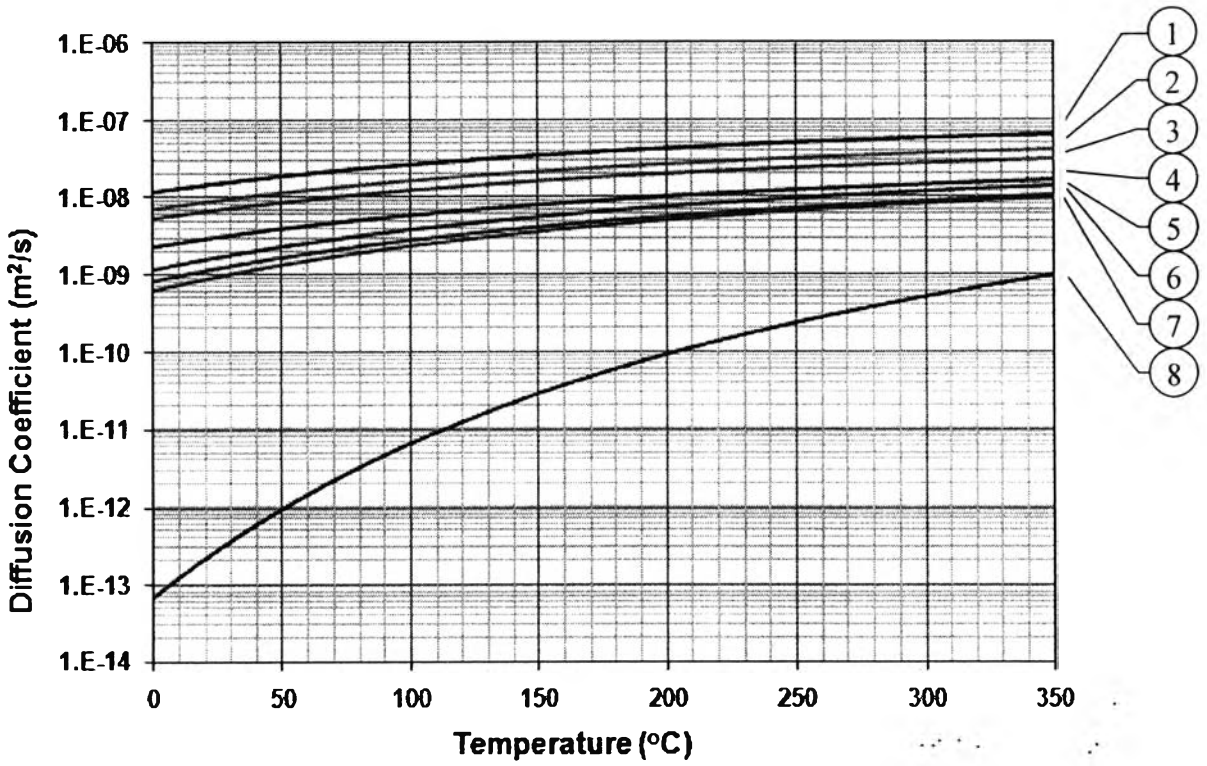

Figure 2.18 Diffusion coefficient of hydrogen through α-iron.

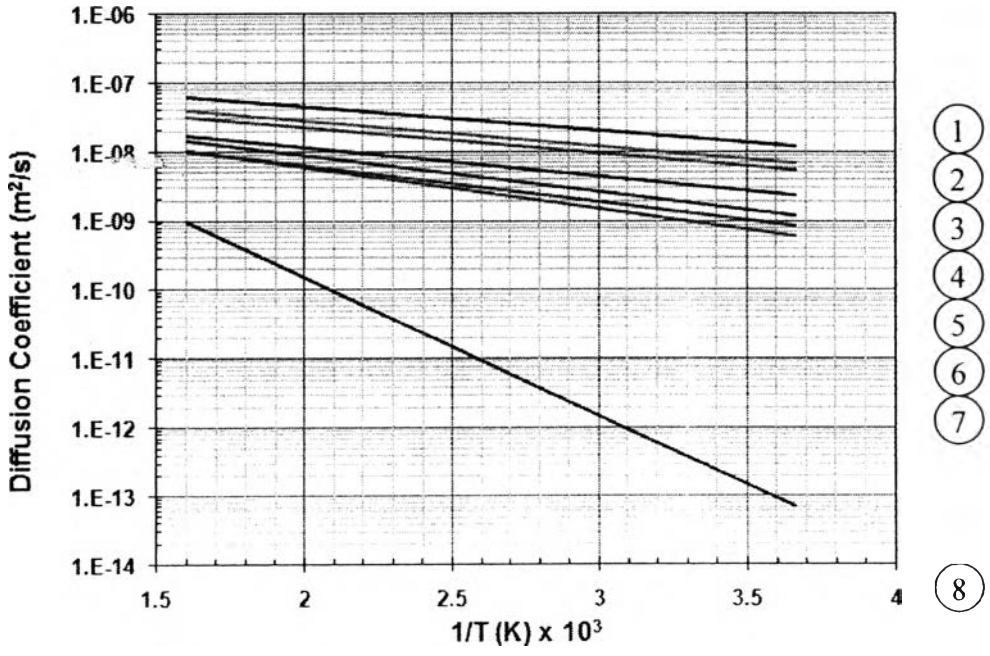

Figure 2.19 Arrhenius plot of hydrogen diffusion coefficient for α-iron.

① $2.33\times10^{-7}\exp\left[\frac{-805.68}{T}\right]$: Nelson and Stein, "Hydrogen in iron" (1978).

② $1.6\times10^{-7}\exp\left[\frac{-851}{T}\right]$: Quick and Johnson, "Hydrogen in iron" (1978).

③ $1.23\times10^{-7}\exp\left[\frac{-848}{T}\right]$: Raczyn'ski, "Corrosion of Metals and Hydrogen-Related Phenomena" (1991).

④ $7.8\times10^{-8}\exp\left[\frac{-956.2}{T}\right]$: Oriani, "Corrosion of Metals and Hydrogen-Related Phenomena" (1991).

⑤ $9.85\times10^{-8}\exp\left[\frac{-1202.8}{T}\right]$: (average) Raczyn'ski, "Corrosion of Metals and Hydrogen-Related Phenomena" (1991).

⑥ $7.5\times10^{-8}\exp\left[\frac{-1219}{T}\right]$: J.Volkl and G.Alefeld, "Diffusion of Hydrogen in Metals" (1978).

⑦ $9.0\times10^{-8}\exp\left[\frac{-1360}{T}\right]$: V.I. Salii, P.V. Gel'd, and R. A. Ryabov, "Permeation, Diffusion, and Solubility of Hydrogen in Pure α-Iron" (1973).

⑧ $1.65\times10^{-6}\exp\left[\frac{-4632.7}{T}\right]$: R.M. Barrer, "Diffusion in and through solids" (1951).

The diffusivity of hydrogen dependences on temperature, that is reported by references ① to ⑦, shows that the values at high temperatures differ somewhat (one order of magnitude). At room temperature, these value differences reach 2 to 3 orders of magnitude. The reasons for this are diverse and it is not easy to determine which one is the major factor. Part of this variation may be due to differences in the iron, extrapolation beyond the temperature, pressure range of measurement etc. Among the possible reasons are surface processes, interaction of hydrogen with linear defects and the development of micro-cracks and blisters in the metal as

induced by hydrogen (J. Flis, 1991). A decrease of the diffusivity of hydrogen in metals because of the attractive interaction with chemical and structural defects is the so-called trapping phenomenon which is important at low hydrogen concentrations (R.A. Oriani, 1994).

Many researchers believe that the reason the diffusivity of hydrogen in iron deviates markedly is due to hydrogen being trapped in lattice defects of the iron at low temperatures. The apparent activation energy in the low temperature region is in the range of 33 to 38 KJ/mol, while in the higher region it is 7.6 KJ/mol (N. Parvathavarthini *et al.*, 2002). Jong-Lam Lee and Jai-Young Lee (1989) studied the behavior of hydrogen in interstitial sites of a normal lattice and in trap sites of iron. The results showed that the apparent hydrogen diffusivities are estimated to be 1×10^{-10} m^2/s for the polycrystalline iron containing only reversible traps (dislocation and grain boundary), and 4×10^{-12} m^2/s for irreversible ones (microvoid). In the case of specimens containing all types of traps such as grain boundary, dislocation, and micro-void, the apparent hydrogen diffusivity is 2.5×10^{-11} m^2/s. For the graph, reference ⑧, which shows a significantly different value of diffusivity, it is believed that there were a large number of traps present in the iron was used in this experiment.

Carbon is always used to strengthen steel. For carbon steel, adding carbon in iron leads to a decrease of the hydrogen diffusion coefficient and hydrogen permeability. In case of additions of 1%wt carbon to Fe-16Al wt%, the results show a decrease in hydrogen permeability and diffusivity by a factor of 2. However, the hydrogen solubility (trapment) in the alloy does not change with carbon addition (W.Y. Choo *et al.*, 1982). An increase in carbon content from 0.045 to 0.085 % has been reported to lead a decrease in the apparent diffusion coefficient of hydrogen by a factor of 8 in 304 stainless steel. Apparently the carbides in the steel lower the diffusional mobility of hydrogen.

Another significant fact is that the diffusivity values depend on the thickness of membranes used. E. Owczarek (2000) performed an experiment to confirm this issue. The results show that the apparent hydrogen diffusivity decreased with the membrane thickness as shown in the Figure 2.20.

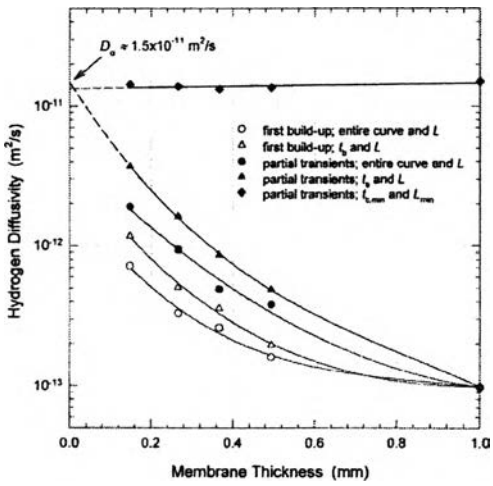

Figure 2.20 The dependence of hydrogen diffusivity on membrane thickness.

In general hydrogen diffusion experiment uses a steel membrane. The membrane is thin and is much less than the thickness of the pipe wall under study which is about 6 mm. Thus it is expected that the diffusivity of hydrogen through a steel pipe wall will be lower than the value from the literature which used a steel membrane.

2.7.4 Hydrogen Permeability in Iron

The permeability constant is defined as the product of the diffusion coefficient (D) and solubility coefficient (S). It represents the amount of a given permeating species which will pass through a given material of unit area and unit thickness under a unit pressure gradient in unit time. There are three controlled variables that have a strong influence on the hydrogen permeation rate; temperature, specimen thickness, and the pressure at the input side of the specimen. Table 2.2 shows a summary of the literature on hydrogen isotope permeability through various materials reported by S.A. Steward (1983). He suggested that the value given by Gonzalez as shown in Equation 2.31 is the most suitable for calculation, because it represents an average of many measurements. Small impurities and grain size seemingly have no significant effect on the permeability of hydrogen through iron.

$$\phi(H_2 / Fe) = 4.1\times10^{-8}\exp\left(\frac{-4200}{T}\right) \quad mol/m\cdot s\cdot Pa^{1/2} \qquad (2.31)$$

Table 2.2 Data of hydrogen permeability in iron (S.A. Steward, 1983)

Φ_0 (10^9 mol/m·s·$Pa^{1/2}$)	E_Φ (K)	Temperature range (K)	Pressure (kPa)	Gas	Reference
4.1	4200	>375	up to 10 MPa	H_2	Gonzalez (1967)
3.58	4100	330-770	10-1000	H_2	Nelson and Stein (1973)
19.5	4700	260-700	20-500	H_2	Louthan *et al.* (1975)
8.13	4700	260-700	20-500	T_2	Louthan *et al.* (1975)
8.63	4300	480-875	10	H_2	Wagner and Sizmann (1975)
6.78	4300	275-335	1-100	H_2	Kumnick and Johnson (1975)
4.98	4217	282-346	1-100	H_2	Kumnick and Johnson (1977)
6.60	4290	322-783	0.4-60	H_2	Quick and Johnson (1978)

In general, the steady-state permeation flux is inversely proportional to thickness for large membranes. As the thickness is reduced the steady-state flux becomes thickness independent.

2.7.5 Hydrogen Diffusivity in Oxide Films

Su-Il Pyun and R.A. Oriani (1989) studied the permeation of hydrogen through passivating films. The results indicate that hydrogen transport through the passivated specimens is significantly retarded by the oxide films in the case of iron. Many years later, P. Bruzzoni *et al.* (1999) indicated that a diffusion coefficient of hydrogen in an oxide layer is very small or several orders of magnitude lower than iron. Therefore most of the hydrogen that is produced at the metal/oxide interface by FAC effuses through the metal, not through the oxide film.

Thin oxide films are shown to be excellent barriers against hydrogen diffusion. The diffusion coefficients of the oxide films are in range of $1.8\text{-}66\times10^{-17}$ cm^2/s while the diffusion coefficient of steel is about 10^{-8} cm^2/s. The value of diffusion coefficient for the oxide depends on its chemical composition, and thickness due to changes in chemical composition of the oxide with thickness. Substrate and oxide grain size had no effect on diffusion rate (M.R. Piggott, 1972).

For studying the hydrogen permeation through metallic samples, a necessary requirement is that the hydrogen permeation rate be controlled by diffusion

in the material of the specimen not by surface reaction. Oxide films, usually present on a metal surface, lower the degree of hydrogen dissociation and the permeation flux. This effect has been attributed to surface phenomena. Significant reductions in the hydrogen permeation rate are achieved even with very thin films. The removal of the surface layers that retard the hydrogen passage from the specimen is a necessary condition for hydrogen diffusivity measurement in metal.

It is common practice to electroplate a thin film of Pd on the specimen to prevent corrosion of the iron or iron-base alloy specimens. The palladium has a very high hydrogen diffusivity and permeability which protects the cleaned surface from oxidation. The diffusion resistance of the Pd layer is so small it does not affect or show-up in the results (D.G. Matei, 1999). Karen Schomberg *et al.* (1996) studied the hydrogen permeation in the passive film on iron formed by chemical polishing. The results indicated that the film is nearly impermeable for hydrogen, even if the hydrogen is in the atomic or protonic state. They suggested that if the oxide films were situated on the hydrogen entry side, the surface reaction or hydrogen dissociation would be strongly retarded and hydrogen uptake would not be possible. On the other hand, hydrogen uptake and permeation of the oxide film may be possible if the hydrogen arriving at the iron/oxide interface is in an atomic/protonic state by coating the surface with palladium.

2.7.6 Hydrogen Diffusivity in Iron Alloys

The hydrogen permeability of Fe alloys has been widely investigated. However, there are relatively few data on the temperature dependence of the hydrogen diffusion coefficient in Fe alloys, and these data are often contradictory.

2.5.6.1 Fe-Al Alloy

Iron aluminides have long been stimulating the interests of material scientists because of their excellent oxidation resistance and relatively low cost and density. There are relatively few investigations to determine the diffusivity of hydrogen in Fe–Al alloys because of a strong tendency to form protective oxides, which impede hydrogen permeation. However, it has been pointed out that the hydrogen diffusivity falls with increasing aluminium content in Fe–Al alloys and the

hydrogen diffusivity is higher in Fe3Al-based intermetallics than in FeAl-based intermetallics (X.Y. Cheng, 2005). In 1997, H. Hosoda *et al.* determined the diffusivity of iron aluminides. They suggested that the lower diffusivity in the iron aluminide containing higher Al is due to the anti-trapping tendency of Al which reduces the effective hydrogen diffusivity (H. Hosoda *et al.*, 1997). However, the attribution of the retardation effect on hydrogen transport in Fe–Al alloys is obscure. Especially, the activation energy of hydrogen diffusion in Fe–Al alloy is not reported (X.Y. Cheng, 2005).

2.5.6.2 Fe-Ni Alloy

Nickel is added to iron to improve its properties because of its permanence in air and its inertness to oxidation. N. I. Shvetsov, *et al.* (1975) investigated the diffusion coefficient of hydrogen in pure iron and Fe-1.5%Ni alloy. They indicated that the addition of 1.5%Ni has little effect on the diffusion coefficient D (and the activation energy of diffusion E_D) of hydrogen. The temperature dependence of the hydrogen diffusion coefficient for the α phase can be described by the equations,

$$D^{\alpha}_{Fe,Ni} = 7.31\times10^{-8} \exp\left(\frac{-1228.6}{T}\right) \ m^2/s \qquad (2.32)$$

. An important aspect of the Fe–Ni alloy system is its structural evolution, with a change from body-centered cubic (BCC) for the Fe-rich alloy to face-centered cubic (FCC) for the alloy with a larger Ni content. J. Völkl and H. Wipf (1981) studied the diffusion of hydrogen in numerous metals. They suggested that the comparison of the hydrogen diffusion in BCC and FCC metals shows as a general rule higher absolute values and lower activation enthalpies for the diffusion coefficient in BCC metals. From their measurements, the results show diffusion coefficients which, at room temperature, are four orders of magnitude larger in the BCC than in the FCC structure, caused by a decrease of the activation enthalpy in the BCC phase by about a factor of 10 against that in the FCC phase.

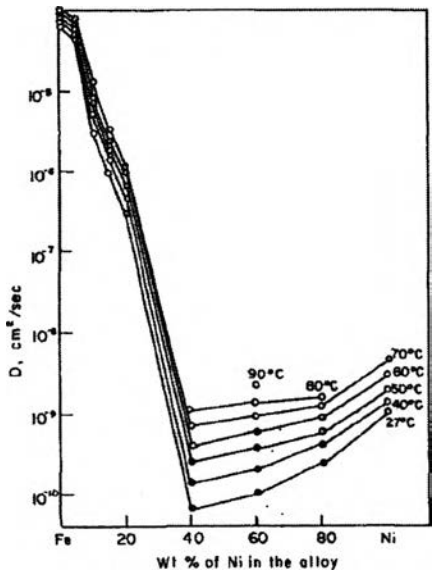

Figure 2.21 Diffusion coefficient of hydrogen as a function of composition at different temperatures (W. Beck *et al.*, 1971).

Hydrogen atoms are transferred between tetrahedral interstices (tetrapores) in BCC metals and between octahedral interstices (octapores) in FCC metals (N.I. Timofeyev, 2006). Consequently, adding more nickel content in iron results in decreasing the hydrogen diffusion coefficient due to the phase change. The values of the diffusion coefficient in the γ-phase are characterized by substantially higher activation energies than in the α-phase. The hydrogen diffusion coefficient dependence on temperature is shown below (J. Völkl and H. Wipf , 1981),

$$D^{\gamma}_{Fe,Ni} = 31.9\times10^{-8} \exp\left(\frac{-4466.3}{T}\right) \text{ m}^2/\text{s}. \qquad (2.33)$$

The study of W. Beck *et al.* (1971) also confirmed that the diffusivity of hydrogen is a function of nickel composition in iron. They indicated that between 0 and 40 wt% of Ni, the dominant factor in controlling the value of the diffusivity is the fall of the mole fraction of the α-phase in the alloy. Between 40 and 100 wt% Ni, the crystallographic phase is all γ, and the major effect is the bonding of hydrogen in the alloy. Figure 2.21 shows the diffusion coefficient of hydrogen as a function of Ni composition.

2.5.6.3 Fe-Cr Alloy

An increase in Cr content can reduce the corrosion rate of steel at high temperatures due to the higher packing density and smaller particle sizes of the oxide layer (Taenumtrakul, 2005). In metallurgy, an iron-carbon alloy with a minimum of 10.5% chromium content is defined as stainless steel. Stainless steel is resistant to corrosion and staining, requires low maintenance, is relatively inexpensive, and has a familiar luster which makes it an ideal base material for a host of commercial applications.

Among the different expressions reported for the dependence on temperature of the diffusion coefficient of hydrogen in austenitic stainless steels, the following expression proposed for a stable 316L in the 23–960 °C temperature range has been selected as shown below (A.-M. Brass *et al.*, 2006),

$$D = 6.2\times10^{-7}\exp\left(\frac{-6450.56}{T}\right)\ \mathrm{m^2/s}. \tag{2.34}$$

The graph in Figure 2.22 shows the hydrogen diffusivities in iron, iron based alloys, and nickel based alloys (Inconel). The first line represents the average value of the hydrogen diffusion coefficient from the literature that was mentioned previously. The next two curves show that the diffusivities of hydrogen decrease when adding nickel, and the extreme decrease when the metal changes its phase from BCC to FCC. The hydrogen diffusion coefficients of inconel and incoloy which are nickel based alloys, are also showed on the graph. Equations of hydrogen diffusivity of inconel and incoloy are shown below (W.M. Robertson, 1977).

$$D_{Inconel\ 718} = 1.07\times10^{-6}\exp\left(\frac{-5992.2}{T}\right)\mathrm{m^2/s}, \tag{2.35}$$

while the diffusivity of hydrogen in Incaloy is

$$D_{Incoloy\ 903} = 2.46\times10^{-6}\exp\left(\frac{-6903.7}{T}\right)\mathrm{m^2/s}. \tag{2.36}$$

The bottom curve representing stainless steel (Fe-Cr alloy) shows the lowest hydrogen diffusivity.

In conclusion, the hydrogen diffusion coefficient of iron-based alloys is several orders of magnitude lower than that of pure iron and becomes less as the

concentration of alloying elements increases due to trapping of hydrogen atoms by alloying elements (K.T. Kim *et al.*, 1981).

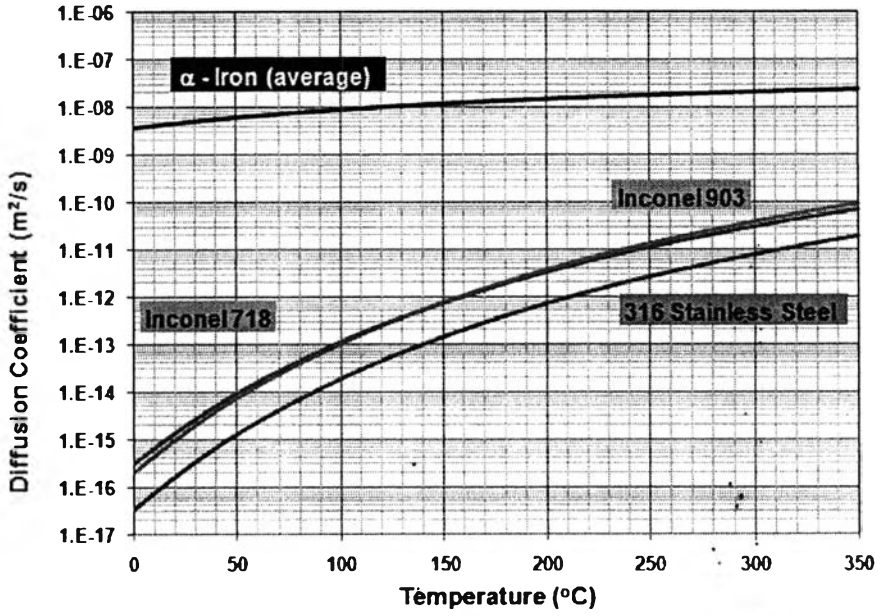

Figure 2.22 Diffusion coefficient of hydrogen through α-Iron and its alloys.

2.8 Hydrogen Solubility in Iron

Hydrogen solubility(s) in the metal represents the quantity of the absorbed hydrogen by a known weight specimen (volume of hydrogen per weight of metal), at a constant temperature and at a constant partial pressure of gaseous hydrogen p_{H_2} after reaching the equilibrium in the system.

The solubility of hydrogen in the regular α structure of iron at temperatures below 300 °C is very slight. V.I. Tkachev *et al.* (1979) found that most of the hydrogen is dissolved in the intergrain matter as shown in Figure 2.23. At temperatures close to room temperature, the solubility of hydrogen in crystalline α structure of grains is 1.28×10^{-5} $cm^3/100$ g.

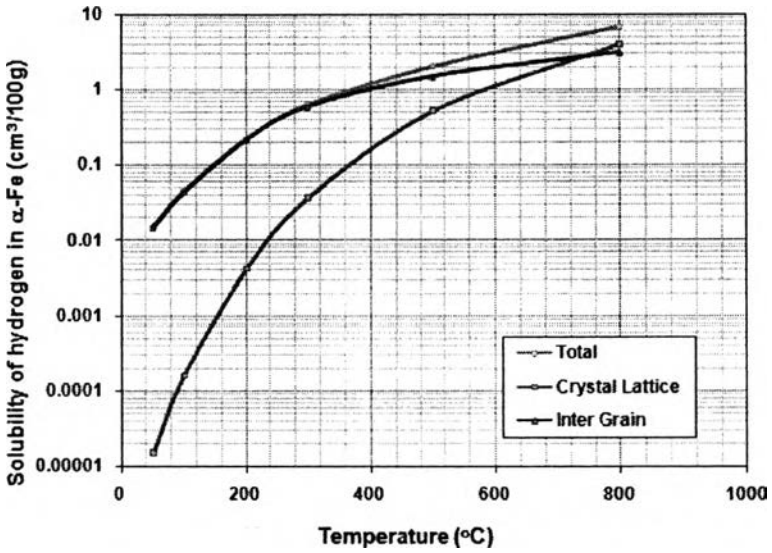

Figure 2.23 Solubility of hydrogen in α-iron (V.I. Tkachev *et al.*, 1979).

In 1981, W. Y. Choo, *et al.* determined the solubility of hydrogen in 99.999% pure α-iron and observed the effect of the alloying elements, such as Mo, W, Ni and Cr on the hydrogen solubility. Figure 2.24 shows hydrogen solubility in pure iron plotted against temperature at one atmosphere from the experiments compare with the value of the lattice solubility of hydrogen in temperature range 400 to 700 °C by Geller and Sun,

$$C(ppm) = 42.7 \times \exp\left(\frac{-27.3kJ/mol}{RT}\right) \tag{2.37}$$

and by Eichenauer (Jong-Lam Lee *et al.*, 1982),

$$C(ppm) = 27.8 \times \exp\left(\frac{-24.4kJ/mol}{RT}\right). \tag{2.38}$$

It was found for the temperatures below 300 °C an abnormally high solubility was observed since the hydrogen solubility should be reduced as the temperature decreases. They suggested that this is caused by the formation of hydrogen traps in the metal. The trapping effect generally starts to show below 300 °C. Therefore it can be concluded that most of the hydrogen in this temperature range exists in trapping sites. The maximum value of hydrogen solubility is observed in the temperature range 80 to 140 °C when the hydrogen concentration is 0.9 ppm.

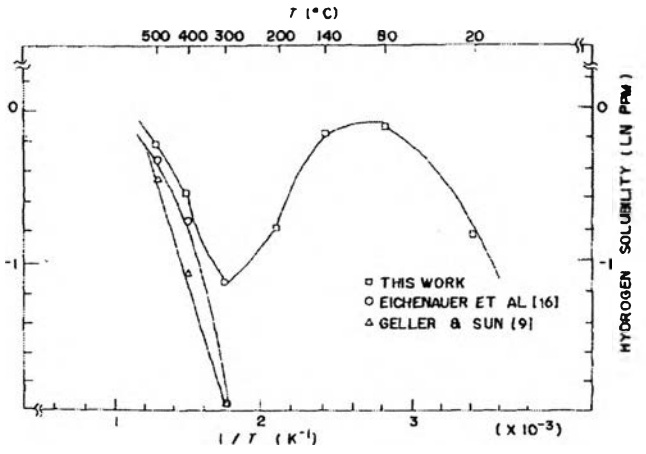

Figure 2.24 Temperature dependence of hydrogen solubility in pure iron at 1 atm pressure (W.Y. Choo *et al.*, 1981).

They also discussed the type of trapping in iron that causes the increase in hydrogen solubility. It was suggested that the hydrogen trapping in dislocations, micro voids, and hydrogen absorption on the surface are disregarded as a possible trapping site in this case. The chemical adsorption of hydrogen in the grain boundary can explain the abnormal behavior of hydrogen solubility below 300 °C.

For the effect of alloying elements on hydrogen solubility, the temperature at which maximum hydrogen solubility is observed and the temperature at which the trapping effect begins increase as alloying elements Mo, W, and Ni are added to the iron. In case of adding Cr, the maximum hydrogen solubility temperature is increased while the critical temperature does not change. These phenomena can be explained by the change of heat chemisorption of hydrogen, and the reduction of the grain boundary area as alloying elements are added.

Studies on the solubility of hydrogen in iron at temperatures below 300 °C (573 K) provide unreliable results due to a low solubility of hydrogen in iron at lower temperatures. its possible interaction with a wide variety of defects in the crystal structure of the metal, and the effect of surface process on the quantities measured. An abnormally high solubility of hydrogen at low temperature was accounted for by

the trapping effect of hydrogen in the metal (J. Flis, 1991). Consequently, the apparent solubility of hydrogen in iron varies with trap density. However, trapping should have little or no effect on the measurable solubility in iron at temperatures higher than 300 °C.

2.9 Hydrogen Damage

Hydrogen damage is a general term which refers to mechanical damage caused by the presence of, or interaction with hydrogen. Hydrogen damage can be classified into four distinct types which are hydrogen blistering, hydrogen embrittlement, decarburization, and hydrogen attack (M.G. Fontana, 1986).

2.9.1 Hydrogen blistering

Hydrogen blistering results from the penetration of hydrogen into a metal. Atomic hydrogen diffusing through metals may collect at internal defects and form molecular hydrogen. High pressures may be built up at such locations due to continued absorption of hydrogen leading to blister formation, growth and eventual bursting of the blister.

2.9.2 Hydrogen embrittlement

The most damaging effect of hydrogen in structural materials is hydrogen embrittlement (HE). Hydrogen-induced cracking (HIC), is the major form of HE and is a brittle mechanical failure caused by penetration and diffusion of atomic hydrogen into the crystal structure of a metal or alloy. Molecular hydrogen formed at those sites builds-up pressure causing the rupture of the inter-atomic bonds, decreasing the cohesive strength, forming voids and blisters that will lead to formation of cracks in the material (D.G. Matei, 1999).

2.6.3 Decarburization and Hydrogen Attack

One of the mechanisms is high temperature hydrogen attack, when hydrogen reacts with carbon and carbides. Hydrogen permeated into the steel can react with carbon, resulting in the formation of methane. The methane is more or less

trapped in the metal structure and will accumulate in voids in the metal matrix. The gas pressure in these voids can generate an internal stress high enough to fissure, crack or blister the steel. This process is known as hydrogen attack and leads to de-carburization of the steel and loss of strength.

The cracking of feeder pipe at PLGS has been studied but there is no evidence that the cracking was due to hydrogen damage. The investigation indicated that the corrosion is caused mainly by FAC. Thus it is expected that the hydrogen atom produced by FAC either diffuses through the pipe wall or into the solution.

2.10 Hydrogen Probe for Monitoring Corrosion

2.10.1 Hydrogen Probe Principle

The concept of the hydrogen effusion probe is based on the fact that one of the cathodic reaction products in the corrosion process is hydrogen. The hydrogen atoms thus generated diffuse through the pipe and are liberated at the exterior surface. Therefore the hydrogen probe can measure the corrosion rate. One advantage of exterior hydrogen monitoring is that it does not require penetration of the pipe wall in order to obtain the corrosion rate since the hydrogen probe is installed outside pipe wall.

It is assume in this method that all of the hydrogen liberated in the corrosion reaction diffuses through the steel vessel wall instead of being liberated as hydrogen gas at the surface. Commercial devices are available for corrosion monitoring by this technique, although it is questionable whether such devices could be positioned and allowed to operate unattended for extended period of time. This method is in also practice limited to steel, which has a high hydrogen diffusivity and low solubility of hydrogen (J.R. Davis *et al.*,1987).

The feeder thinning occurs because iron atoms (Fe^{2+}) in the steel dissolve into the coolant as a consequence of FAC. The hydrogen probe can measure the pipe thinning rate since the quantity of hydrogen effusing through the carbon steel pipe is proportional to the rate that iron is lost into solution. It is assumed that one mole of hydrogen gas is produced from one mole of iron ion losses. The reaction for this relation is shown below.

$$Fe + 2H^{+} \rightarrow Fe^{2+} + 2H \tag{2.39}$$

The hydrogen probe system operates under vacuum. In principal, hydrogen effusing from the pipe would be collected in the chamber outside of the pipe wall and cause the pressure to rise. The pressure transducer or pressure gauge would measure the hydrogen pressure increase which could be used to calculate wall thinning rates.

An important feature of hydrogen flux probe monitoring is that it is a real-time device, which can detect short-term upsets in the process. By getting near real-time data from a corrosion monitoring, operators can relate this data to events that caused the corrosion. Then they can lower corrosion rates by adjusting or eliminating corrosion-causing events.

The rate of corrosion is related to hydrogen evolution based on Equation 2.40. One mole of H_2 is produced for one mole of Fe^{2+} loss.

$$Fe + 2H^{+} \rightarrow Fe^{2+} + 2H \tag{2.40}$$

The rate of corrosion can be determined from the accumulation of hydrogen molecules according to following equation.

$$C = \frac{a\frac{\partial n}{\partial t}M}{A\rho} \tag{2.41}$$

Where C is corrosion rate (cm/yr), M_{Fe} is molar mass of iron which is 55.85 g/mol, A is internal area of pipe (cm^2), ρ_{Fe} is the density of iron which is 7.86 g/cm^3, a is the conversion of days to year (365 days/yr), and $\frac{\partial n}{\partial t}$ is a daily accumulation of hydrogen molecules in a unit of moles/day.

Since hydrogen behaves as an ideal gas at low pressures, the number of moles of hydrogen accumulation per day can be related to the change in pressure by the ideal gas law.

$$\frac{\partial n}{\partial t} = \frac{\partial P}{\partial t}\frac{V}{RT_{eff}} \tag{2.42}$$

Where $\frac{\partial P}{\partial T}$ is the rate of pressure increase in Pa/day. V is total volume of the HEP which depends on an assembly of the HEP, R is gas constant (8.314 m^3·Pa/mol/K),

and T_{eff} is the effective temperature (K) in the system. Since various parts of the HEP system are exposed to different temperatures, the effective temperature therefore is the sum of the individual temperature multiply by their respective volume percentage of the HEP system.

2.10.2 Comparing HEP to FOLTM (Conventional Device)

Another device that can be used to measure the feeder thinning rate is called Feeder On-Line Thickness Monitor (FOLTM). FLOTMs have been used in the CANDU industry for the past 8 years to measure actual feeder thickness. The first FOLTM installation at Point Lepreau nuclear station was in January, 1998. It works by using ultrasonic transducers. These transducers can directly measure pipe wall thickness, average fluid temperature, and fluid flow. The FOLTM multi-sensor continuously measures wall thinning and fluid temperature and then inputs these parameters in the flow measurement, because flow measurement accuracy relies on pipe internal diameter and fluid temperature (K. McKeen *et al.*, 2007).

Both the FOLTM and the HEP are devices that can be used to measure the feeder wall thinning, and do not require penetration of the pressure boundary since it is mounted externally. However, the FOLTM and the HEP are based upon different principles. While the FOLTM provides a measurement of feeder wall thickness, the HEP provides a measurement of apparent change in wall thickness. However, the signal-to-noise ratio of the HEP is much higher than that of the FOLTM. Consequently, the HEP can measure apparent feeder wall thickness rates over much shorter times; hour versus week. Thus, unlike the FOLTM, the HEP is capable of monitoring apparent feeder wall thinning rates during short-term operating transients, and is capable of measuring abrupt changes in feeder wall thinning rate.

2.11 Former Experiments on the Hydrogen Probe

2.11.1 Hydrogen Patch Probe

The hydrogen patch probe was first patented in 1992 by H. Bruce Freeman. The apparatus comprises a chamber-defining member which is constructed of material sufficiently flexible and can be sealed to the pipe. A vacuum gauge is

used to monitoring the decay of the vacuum in the chamber over time. Yépez *et al.* (1998) used this apparatus to compare a vacuum loss method and a conventional electro chemical technique. The experimental results showed that the transient response of a vacuum based hydrogen probe provides similar information regarding the hydrogen diffusion through steel walls compares to the conventional electro chemical technique. However they suggested that the electrochemical technique tends to be more accurate for detecting small hydrogen fluxes in the laboratory but may be more difficult to apply in the field than the vacuum based method.

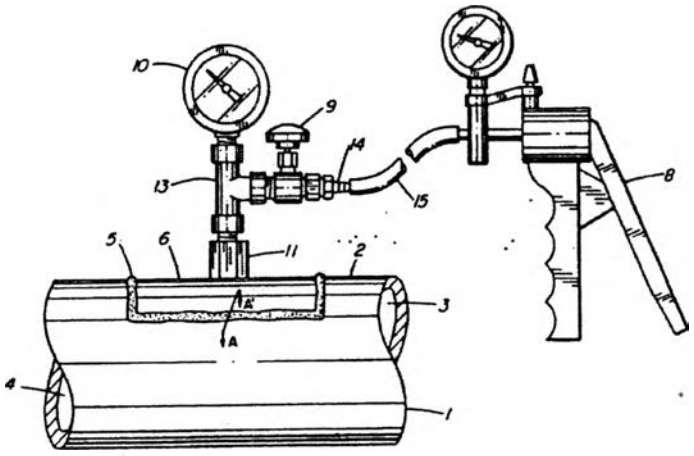

Figure 2.25 Hydrogen patch probe configurations (H. Bruce Freeman, 1994).

2.11.2 Hydrogen Vacuum Foil or Beta Foil

In 1999, D.G. Matei studied the new method for monitoring corrosion called a hydrogen vacuum foil. The hydrogen vacuum foil (Beta Foil) consists of a thin stainless steel foil which is attached to a length of capillary tube and the foil is applied directly onto the surface of the pipe or vessel to be monitored. The Beta Foil configuration is presented in Figure 2.26. The results from this work indicated that the amount of hydrogen permeating through the steel specimen is a function of the material and the environmental conditions and not a function of the capillary tube length. It is suggested that the vacuum under the Beta Foil should be maintained above -20 kPa in order to obtain accurate measurements. For a lower vacuum, the Beta Foil is fairly insensitive to the changes that occur in the system. Moreover, the

vacuum foil technique should not be used where oxygen is present in the corroding system since the hydrogen reduction reaction is no longer the dominant reaction and the measurement of hydrogen permeating through the steel specimen is no longer reflective of the corrosion rate. Thus the Beta Foil technique is the limitation of its use in aerated conditions.

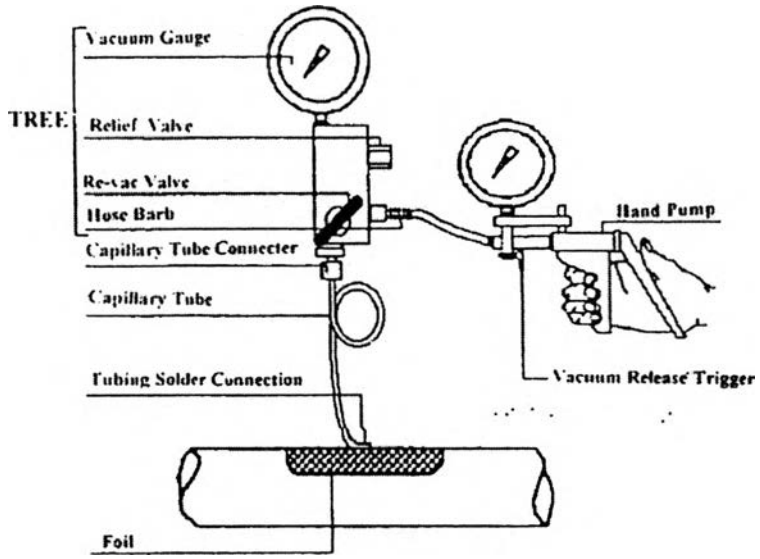

Figure 2.26 Beta Foil configurations (D.G. Matei, 1999).

2.8.3 Hydrogen Effusion Probe (HEP)

The HEP consists of silver cup connected via silver and stainless steel tubing to a valve, pressure transducer, vacuum pump, and data acquaintance system. In order to avoid the leaking of hydrogen from the device, high purity silver is used due to the low permeation rate of hydrogen through this metal at high temperature. The system temperature is measured by installed thermocouples. The main components of the HEP instrumentation unit are an isolation valve, a precision absolute pressure transducer, and a data acquisition and control system. The pressure transducer has a controlled internal temperature of 45°C and a limiting ambient operating temperature of 40°C. Changes in ambient temperature affect the transducer reading. The data acquisition and control system is used to control the pump and valve opera-

tion, and also record readings from the transducer and thermocouples. The thermocouples provide temperature information to enable analysis of the data.

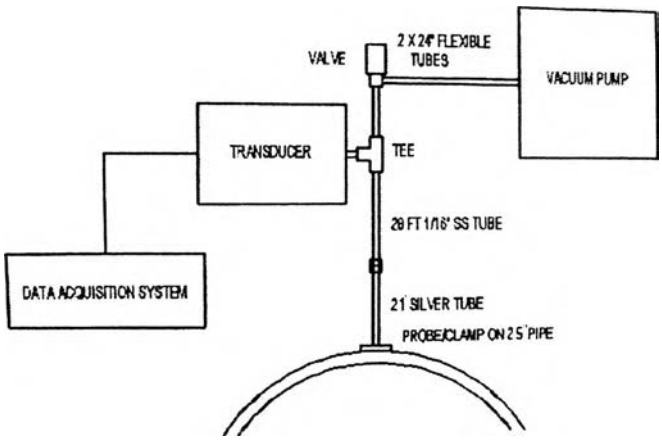

Figure 2.27 Schematic of HEP Assembly (K. McKeen *et al.*, 2007).

It was expected that after a predetermined pressure is reached, 2000 Pa is recommended as the pressure range that is independent of hydrogen pressure, the data acquisition and control system would automatically repeat the test cycle. The vacuum pump would switch on to evacuate the measuring volume and restart the cycle (K. McKeen *et al.*, 2007).

Since 2001, Atomic Energy of Canada Limited (AECL) has performed a series of loop experiments funded by the CANDU® Owners Group Inc. (COG). The objective of this experiment is to study the FAC process that causes feeder wall thinning in the primary heat transport system of CANDU reactor. The results demonstrate that the rate of the FAC process in the tube can be examined online by measuring the rate of hydrogen that is produced from FAC process, which effuses through the pipe wall. Consequently, this information led to the development of a Hydrogen Effusion Probe for monitoring of FAC.

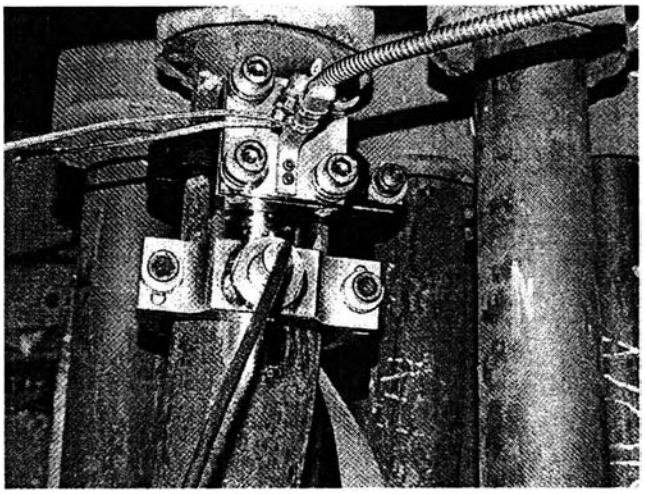

Figure 2.28 The HEP (top) and FOLTM (bottom) installed on feeder pipe at PLGS (K. McKeen *et al.*, 2007).

In 2006, the Centre for Nuclear Energy Research (CNER) has been conducting HEP experiments. The objective of this project was to design and build an HEP that could be installed on an outlet feeder pipe at the Point Lepreau Generating Station (PLGS) and water wall tubing at the Coleson Cove Generating Station (CC). Figure 2.28 shows the HEP installed on a feeder pipe at the PLGS. Leak tests of the HEP were performed prior to start-up, and leak rates of 5 Pa/day which represents only a 0.25% contribution were determined. Data from the PLGS indicate that the HEP can provide an on-line indirect measurement of the feeder wall thinning rate which is approximately 60 μm/year. This feeder wall thinning rate can be compared with the rate measured by the FOLTM, which was installed next to the HEP for the same period of time. The data indicated that the feeder wall thinning rate from both devices was in agreement.

Although the accuracy of this rate has not yet been quantified, the feeder wall thinning rate is consistent with the expected rate for a straight length of outlet feeder pipe. The data from this experiment also suggest that the HEP is able to detect small changes in the FAC rate over short periods of time. The ability to monitor not only the corrosion of carbon steel outlet feeder pipe but also changes to the reducing/oxidizing (redox) chemistry may be possible.